Radio Science, Volume 36, Number 1, Pages 79–96, January–February 2001

Determination of source thunderstorms for VHF emissions observed by the FORTE satellite

Heidi E. Tierney,[1,2] Abram R. Jacobson,[1] William H. Beasley,[3] and Paul E. Argo[1]

Abstract. This paper explains a method of locating groups of satellite-observed VHF signals from lightning that emanate from isolated storm regions. LF/VLF signals recorded and located by the National Lightning Detection Network (NLDN) are often accompanied by broadband VHF emissions of sufficient intensity to trigger satellite-based RF receivers. It has previously been shown that events recorded by the FORTE satellite and the NLDN, which have occurrence-time differences of 0.3 ms or less, can be assumed to originate at the same approximate geolocation with 97.5% reliability. For such event pairs, the VHF events recorded by FORTE were assigned the NLDN locations. We use graphical analysis to identify groups of satellite data that can be assumed to originate from the same storms as the located events. To accomplish this, a value of total electron content (TEC) is derived from the frequency dispersion of each VHF signal recorded by FORTE. Scatterplots of TEC versus time often reveal curved clusters of satellite data. The variation of TEC with satellite elevation angle, and time, is consistent with a model in which the length of a signal's required propagation path through the ionosphere changes with satellite and storm position. We use the values of TEC for the located satellite data, a simple model of the ionosphere, and NLDN data to help us identify TEC clusters that can be assumed to originate from relatively compact, and unambiguous, geolocations. For the time period of April through September of 1998 we geolocate 65 groups of satellite data records. A total of 6131 satellite data records, which were not previously located, have been assigned the median NLDN coordinates of their corresponding storm.

1. Introduction and Background

Using RF receivers on satellite platforms, researchers at Los Alamos National Laboratory (LANL) have undertaken the study of VHF (20-300 MHz) signals from lightning. These signals must travel through the lower neutral atmosphere and the ionosphere before they are recorded by a satellite instrument. Water vapor and clouds in the lower atmosphere do not appreciably attenuate signals in this frequency range, and the primary effect of the ionosphere is to disperse the signals with a frequency-dependent group delay. The total electron content (TEC), which is the integral of the electron density over the path that a signal takes to a satellite, can be derived from the observed frequency dispersion.

The FORTE satellite is in a circular orbit at an altitude of about 800 km. This orbit has a 70° inclination with respect to the Earth's equator. It covers equatorial regions and midlatitudes, the most important lightning-producing regions of the globe. FORTE observes VHF emissions from lightning, or other sources, that originate within a circle of greater than 3000-km arc radius centered at satellite nadir. This limit of FORTE's VHF horizon is an approximation from a geometric model and is confirmed by observation.

With a single VHF receiver and no location information from an independent system, signals recorded at FORTE can only be located to within the

[1]Los Alamos National Laboratory, Los Alamos, New Mexico.

[2]Also at Department of Physics and Astronomy, University of Oklahoma, Norman.

[3]School of Meteorology, University of Oklahoma, Norman.

Paper number 1999RS002254.
0048-6604/01/1999RS002254$11.00

satellite's footprint. *Jacobson et al.* [2000] were able to assign more definite locations to 14,985 satellite signals with the use of "relaxed criteria" data provided by the National Lightning Detection Network (NLDN). These authors examined the occurrence-time statistics for events recorded by both the NLDN and FORTE. NLDN locations were assigned to FORTE VHF signals that occurred within 0.3 ms of LF/VLF waveforms located by the NLDN. The NLDN relaxed-criteria data set and the time-correlation method of locating satellite data are explained in section 2 and section 3, respectively.

We use the derivable quantity TEC (section 4) to help identify groups of satellite data that originated in the same storms as the 14,985 FORTE signals that were assigned locations. Consider a situation in which a few compact storms, within the satellite's footprint, are simultaneously active. VHF signals from each storm will take unique paths through the ionosphere to the satellite and can be assigned values of TEC. In many cases the values of TEC from the separate storms will form separate clusters in plots of TEC versus time. It is our goal to assign a median location to all members of such clusters. We first require that a given cluster can be attributed to only one storm observed by the NLDN. To do this, the located events and their measured values of TEC are used to estimate the ionospheric conditions during the satellite observation run of interest. Using a simple model of the ionosphere, the paths from the relaxed-criteria NLDN locations to the satellite can then have theoretical values of TEC assigned to them. A comparison of the theoretical plots of TEC versus time with the plots of satellite data helps us eliminate cases where more than one storm produces a single TEC cluster (section 5). In addition, we select storms that are contained within ±2.5° in latitude and longitude. The relaxed-criteria NLDN data are used to determine the storm size, which gives us a measure of the location uncertainty. Herein we have determined the source thunderstorms for 65 TEC clusters of VHF data records observed by FORTE. We have assigned a median storm location, as given by the NLDN, to the nonlocated events of each cluster.

The study of lightning using satellite-based VHF receivers at LANL began with the discovery of transionospheric pulse pairs (TIPPs). TIPPs were first observed in 1993 with a VHF receiver, called Blackbeard, on board the ALEXIS satellite [*Holden et al.*, 1995]. TIPPs are distinguished from other naturally occurring radio emissions by several features [*Massey and Holden*, 1995]. TIPPs consist of exactly two broadband (25-100 MHz) pulses that have been dispersed by the ionosphere. The duration of each pulse is a few microseconds, and the time separation of the pulses is typically tens of microseconds. Using Blackbeard, the peak power of either pulse in a TIPP was found to be stronger than the peak VHF power of return strokes from cloud-to-ground (CG) lightning. However, the triggering mechanism of Blackbeard requires only that the instantaneous power within a 75-MHz bandwidth reach a selected level. Because of this, it is necessary to set the triggering power level high in order to reduce the number of narrowband signals recorded. TIPPs have been the primary focus of lightning studies using Blackbeard. Since the discovery of TIPPs, some evidence has supported the hypothesis that the two pulses of the pair are the direct and ground-reflected signals from a thunderstorm source [*Holden et al.*, 1995; *Jacobson et al.*, 2000; *Massey and Holden*, 1995; *Massey et al.*, 1998; *Smith*, 1998]. A model in which two temporally linked VHF sources of thunderstorm origin are responsible for the production of TIPPs has also been presented [*Roussel-Dupré and Gurevich*, 1996].

A second satellite carrying optical and RF instruments, FORTE, was launched on August 29, 1997. FORTE carries two RF receivers, both of which are described in detail by *Jacobson et al.* [1999]. The receiver used in this study has two passbands; each is independently tunable in the range of 20-300 MHz with 22-MHz effective bandwidth. Both of the passbands have eight subbands of 1-MHz bandwidth that trigger independently. This design was implemented so that the receiver would trigger off of wideband signals and discriminate against carriers. The trigger threshold for each subband can be set at a fixed level or at a selected decibel level above the noise background. For a signal to be recorded it is typically required that five out of eight of the subbands trigger within a several microsecond coincidence window. Using this triggering scheme, a variety of broadband VHF signals from lightning, including TIPPs, have been recorded.

To date, the satellite has recorded about 2.6 million events. Much of what we have learned about these events has been through time correlation with events located by the NLDN. Recent studies have

shown that many of the LF/VLF waveforms of lightning return strokes and cloud pulses observed by the NLDN correlate in time with VHF signals observed by FORTE. For example, optical and VHF signals recorded by FORTE that are time-coincident with type-classified NLDN waveforms have been analyzed by *Suszcynsky et al.* [1999]. With better than 90% confidence, these authors were able to distinguish between the NLDN designations of return stroke, subsequent return stroke, and intracloud discharge based on the satellite-recorded VHF signature. This result suggests that satellites can be used to examine discharge-type statistics in regions outside of areas covered by ground-based sensors.

Other authors have used time-correlation analysis to investigate the source of TIPPs. TIPPs were found to correlate in time with LF/VLF intracloud pulses observed by the NLDN [*Jacobson et al.*, 2000; *Zuelsdorf et al.*, 1998]. *Cummins et al.* [1998] report that some of the relatively intense, longer-duration intracloud discharge events may be the same class of event as the isolated, positive bipolar pulses identified by *Weidman and Krider* [1979]. Because the bipolar pulses are accompanied by intense noise-like bursts of radiation [*Le Vine*, 1980; *Willett et al.*, 1989], it has been suggested that these events are the source of the first pulse of a TIPP [*Smith*, 1998].

Using time coincidence techniques alone, only a few percent of the events recorded by the satellite are assigned locations. Many more events can have their locations approximated if it can be determined that they occurred in the same storm, or flash, as the time coincident events. For cases where this is possible, we will be better able to study the geographic and temporal characteristics of satellite observations of TIPPs, cloud discharges, and cloud-to-ground discharges.

2. NLDN Data

The method of locating events presented herein is largely dependent on coincidences between the time of occurrence of LF/VLF radiation field signals recorded by the NLDN and the time of occurrence of VHF lightning signals recorded by FORTE. Standard, quality-controlled NLDN data provide locations of cloud-to-ground lightning return strokes within 625 km of the nearest participating NLDN station. The overall detection efficiency for first return strokes and subsequent return strokes is about 80-90%. For this standard data set, return stroke events with peak currents exceeding 5 kA are located with a median accuracy of 500 m [*Cummins et al.*, 1998]. *Jacobson et al.* [2000] caution that events classified as positive CG strokes with peak currents less than 10 kA may be misidentified cloud pulses.

The NLDN data used in this study were obtained with relaxed criteria. This allowed for more time coincidences with FORTE observations than was possible using only the standard data. In addition to the standard data, this data set provides locations for energetic cloud discharges occurring within or near the network, distant CG discharges, and discharges that are not type classified [*Jacobson et al.*, 2000]. The relaxed-criteria data are not located with the accuracy obtainable for high-current return strokes occurring within the network. Events classified as cloud discharges have a location accuracy of better than 3 km [*Jacobson et al.*, 2000]. Any impulsive waveform with a peak-to-zero time of less than 10 μs is classified as a cloud discharge. Lightning discharges occurring 2000-4000 km outside of the United States have an error of 16-32 km in their assigned NLDN coordinates [*Cramer and Cummins*, 1999]. Peak currents of discharges with sources greater than 625 km beyond the nearest participating NLDN station were set to zero and thus are not type classified. Beyond this range the ionospheric reflection of the sky wave can be stronger than the ground wave, and hence source strength estimates based on ground wave propagation may not be valid. The relaxed-criterion data set also contains numerous "outlier" events which have location errors of greater than or equal to 50 km [*Jacobson et al.*, 2000].

3. NLDN/FORTE time coincidences

As explained in section 1, lightning events observed by FORTE include VHF from leader processes, first return strokes, and energetic cloud pulses. *Jacobson et al.* [2000] showed that signals detected at the FORTE satellite with source times within 0.3 ms of the times assigned to discharges located by the NLDN can be assumed to originate at the approximate NLDN location with an estimated 97.5% reliability. This study included data from FORTE and the NLDN covering April through September of 1998. The time difference of 0.3 ms was chosen to be significant as follows. First, NLDN

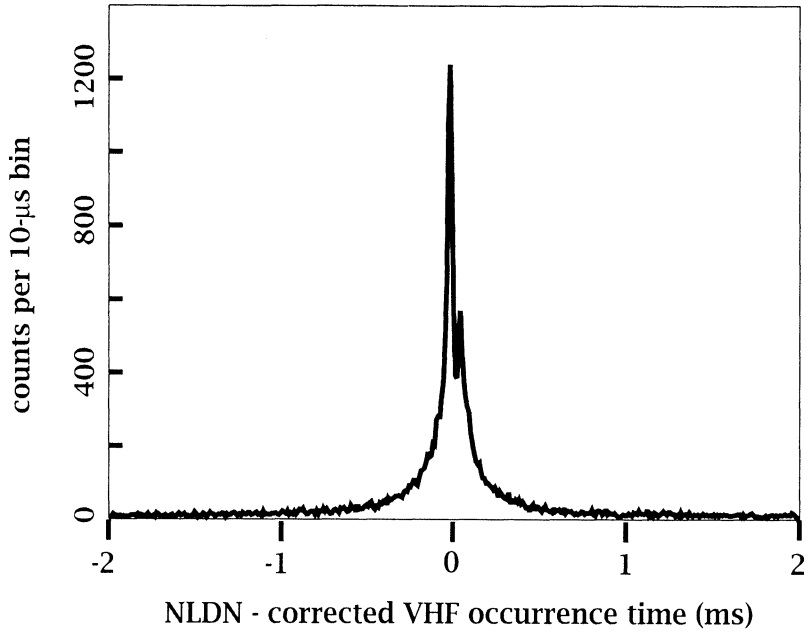

Figure 1. Histogram of the difference between the National Lightning Detection Network (NLDN) stroke time and the corrected FORTE event time, with a 10-μs bin size. The flat pedestal outside of ±0.3 ms is featureless and due to accidental coincidence. Adapted from *Jacobson et al.* [2000].

locations were assigned to FORTE events that were detected within ±200 ms of an NLDN-located stroke. For each of these events, the time of flight from the test location to FORTE was subtracted from the time that the event was detected at FORTE. This gave putative occurrence times for the FORTE events. The occurrence-time difference (NLDN – FORTE) was then found and a histogram of these time differences was plotted over a time range of –200 to +200 ms. A total of 14,985 out of 261,023 satellite events were shown to have occurrence times within ±0.3 ms of the NLDN given occurrence time (Figure 1). These 14,985 events form a statistically significant central peak. A background, or noise, level is estimated outside of this central peak where the histogram is flat. Each 1-ms bin outside of the central peak contains 616 events that are not as closely correlated in time. If we assume that these coincidences are by chance, this implies a contamination of 369 misidentified events within the ±0.3-ms central peak. Hence 97.5% of the events within the statistically significant peak are above the background level and are assumed to be reliable. These events were assigned the coordinates of their time-corresponding NLDN events, and we will refer to them hereinafter as "prompt coincidences."

Jacobson et al. [2000] examined the 14,985 prompt coincidences to determine which type of NLDN discharge was most often closely time coincident with FORTE. The numbers per type are as follows: 7353 untyped, 4083 negative CG, 2882 positive CG, and 665 intracloud discharges. For each type, the number of events detected by FORTE was compared with the total number of events, lying within FORTE's 3000-km range, detected by the NLDN. It was shown that intracloud discharges are about 10 times more likely, and positive CG discharges are about 5 times more likely, to produce a detectable VHF emission than negative CG discharges. These authors studied other relationships among the NLDN type-classified events and the time coincident observations made by FORTE.

4. Total Electron Content

The data analyzed in this paper were obtained with FORTE's receiver tuned to a low frequency band (26-48 MHz). Using the following method,

each 400-μs recording of digitized electric field data was assigned a value of TEC. First, a fast Fourier transform (FFT) is repeatedly applied to 2.56-μs windows of each data record in steps of 0.16 μs. Thus every 400-μs data record gets transformed into about 2500 spectrograms with frequency resolution of 0.39 MHz. Each spectrogram contains information of the average electric-field spectral density $[(V/m)^2/MHz]$ as a function of frequency. When the spectrograms of each record are displayed as a time series, we refer to the result as a periodogram. The periodograms are plots of electric-field spectral density as a function of frequency and time. Impulsive RF signals that have traveled through the ionosphere and have energy that spans much of the frequency range from 26 to 48 MHz exhibit dispersion.

This dispersion is a frequency-dependent time delay that can be attributed to four physical processes. *Massey*, [1990] derived analytical expressions for these time delays using a slab ionosphere model. The leading order effect is a delay due to the presence of plasma. Group delays due to magnetic interactions, the particular distribution of the electron density along the path, and refraction are higher-order corrections to this delay. For the ionosphere the time delay τ of a frequency group can be approximately expressed as a function of the TEC traversed (electrons/m^2) and the frequency f (hertz) of the group.

$$\tau(\text{sec}) \cong \frac{k \times \text{TEC}}{(f \pm f_c \cos\alpha)^2}. \qquad (1)$$

Above, using the International System of Units (SI), k has a constant of value 1.34×10^{-7}. The electron cyclotron frequency for the ionosphere is denoted f_c. Its product with cos α, where α is the angle between the propagation vector and the Earth's magnetic field, typically has a value of less than 1 MHz and is neglected in this analysis. We note that at low elevation angles, corrections from refractive bending can become more important than the magnetic correction.

Using Eq (1), the TEC traversed by each VHF signal can be estimated as explained by *Jacobson et al.* [1999]. We describe the process briefly here. For each periodogram the TEC is varied over a regular grid of trial values. For each trial value of TEC the expected time delay of every frequency group is calculated. The expected time delay is then subtracted from the arrival time of each frequency group. One trial value of TEC best corrects the observed dispersion such that it appears that all frequencies arrived at the antenna simultaneously. To test this quantitatively, the frequency integral of the time-corrected electric field spectral density is performed for each time column of the periodogram, and this quantity is taken to the fourth power. These results, one value for each time step, are then summed over time. This time sum of the fourth power of the intensity is a maximum for the best value of TEC. The optimum value of TEC is then recorded and used in the following analysis.

4.1. Variation in TEC With Elevation Angle

We now present two simple models of the ionosphere that demonstrate the variation in TEC with satellite elevation angle. Consider Figure 2a. In this plane-parallel model, θ is the elevation angle. It is measured between a line tangent to the surface of the Earth and a line joining the storm location and the satellite. The smaller the elevation angle is, the greater is the slant path of the ionosphere through which the signal has to travel before reaching a satellite. For this simple model the TEC is a maximum when the elevation angle is a minimum. As the satellite approaches the storm, the TEC decreases, and when the satellite is at closest approach to the storm the TEC is a minimum. In cases where a satellite observes an active, isolated storm for several hundred seconds, the observed variation in TEC is often consistent with a change in slant path as the satellite moves over the storm. In addition, if several storms are simultaneously active, the elevation angles from the different sources to the satellite may be different. This difference is often great enough such that the derived values of TEC can help separate the signals of one storm from another.

For a simple plane-parallel model of the ionosphere (Figure 2a) the slant path TEC observed by the satellite can be approximately modeled using the following equation:

$$\text{TEC} = N_e s = N_e t / \sin\theta. \qquad (2)$$

In (2), N_e is the free electron density, s is the slant path, t is the thickness of the ionosphere, and θ is the elevation angle.

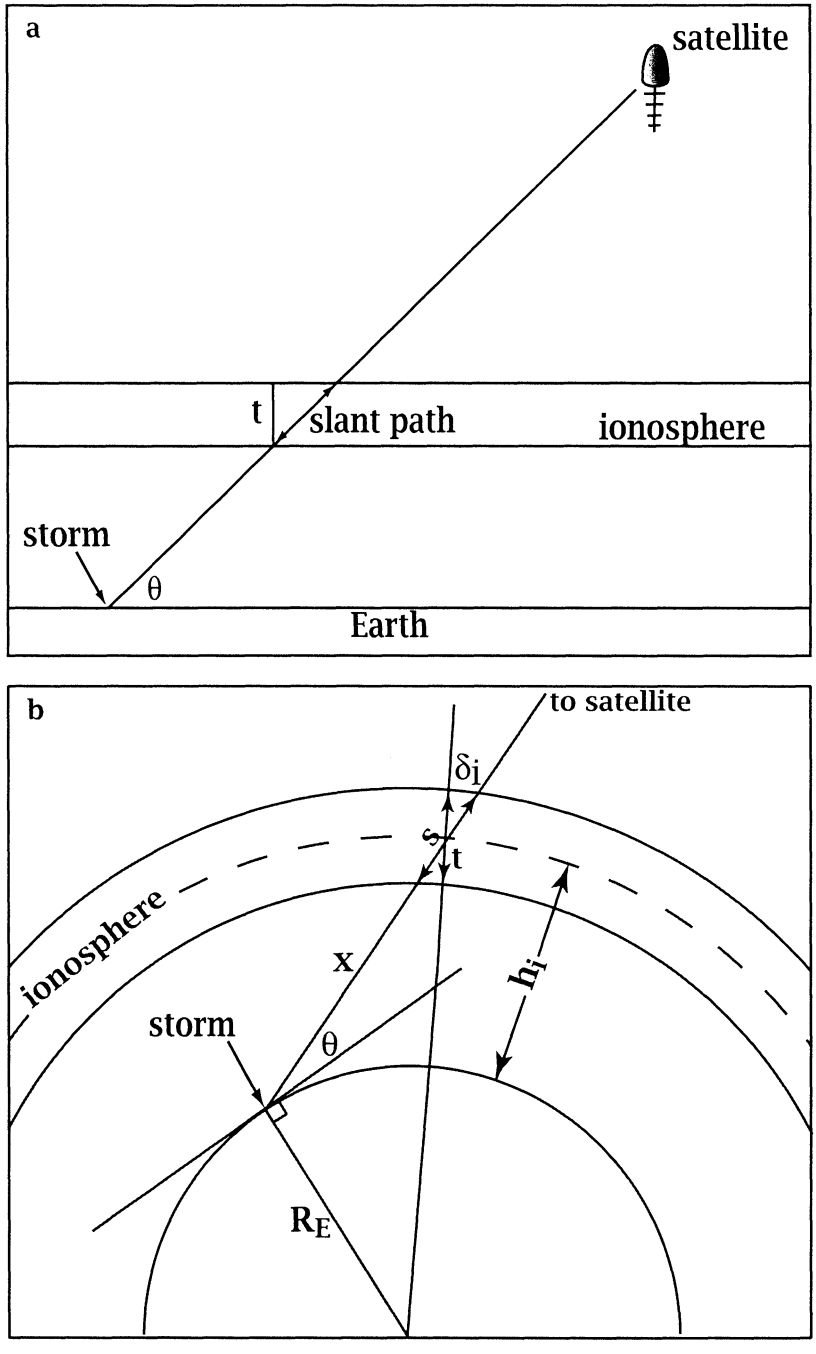

Figure 2. These simple models illustrate how the slant path, traversed by storm-emitted VHF signals, can change during a satellite pass over a storm.

For comparison, we consider a spherical Earth model in which the ionosphere is assumed to be planar in the region where it is intersected by the ray path (Figure 2b).

$$\mathrm{TEC} = N_e s = \frac{N_e t}{\cos \delta_i} \tag{3}$$

$$\delta_i = \cos^{-1} \frac{\left(x^2 + (R_E + h_i)^2 - {R_E}^2\right)}{2x(R_E + h_i)}$$

$$x = R_E \cos(\theta + \pi/2) + \left[\left(R_E \cos(\theta + \pi/2)\right)^2 - \left({R_E}^2 - (R_E + h_i)^2\right)\right]^{1/2}.$$

In these equations, δ_i is the zenith angle for the ray path at the height of the ionosphere, h_i. R_E is the radius of the Earth, and x is the distance from the storm to the central altitude of the ionosphere along the ray path.

In both of these models the ionosphere is assumed to have uniform electron density. The real ionosphere has two dominant layers, the E and F layers, which both have an electron density that varies with height. The peak of the electron density in the E layer is typically at an altitude of 100-110 km. The more heavily ionized F layer has a peak electron density at an altitude that varies in the range of 200-400 km [*Budden*, 1988]. The magnitude and distribution of the electron density vary with time of day, latitude, solar cycle, and season. To attempt to model the various ionospheric conditions that the satellite passes over would be difficult. Furthermore, the dominant cause of the group delay is from the presence of the electron plasma and not its detailed structure. Thus we find it reasonable to apply these simple models by estimating a value for the quantity $N_e t$.

We compare the mean behavior of slant path TEC versus elevation angle for the located satellite data to the two models. For the 11,194 of the 14,985 prompt coincidences, we plot the mean slant path TEC as a function of satellite elevation angle for both night

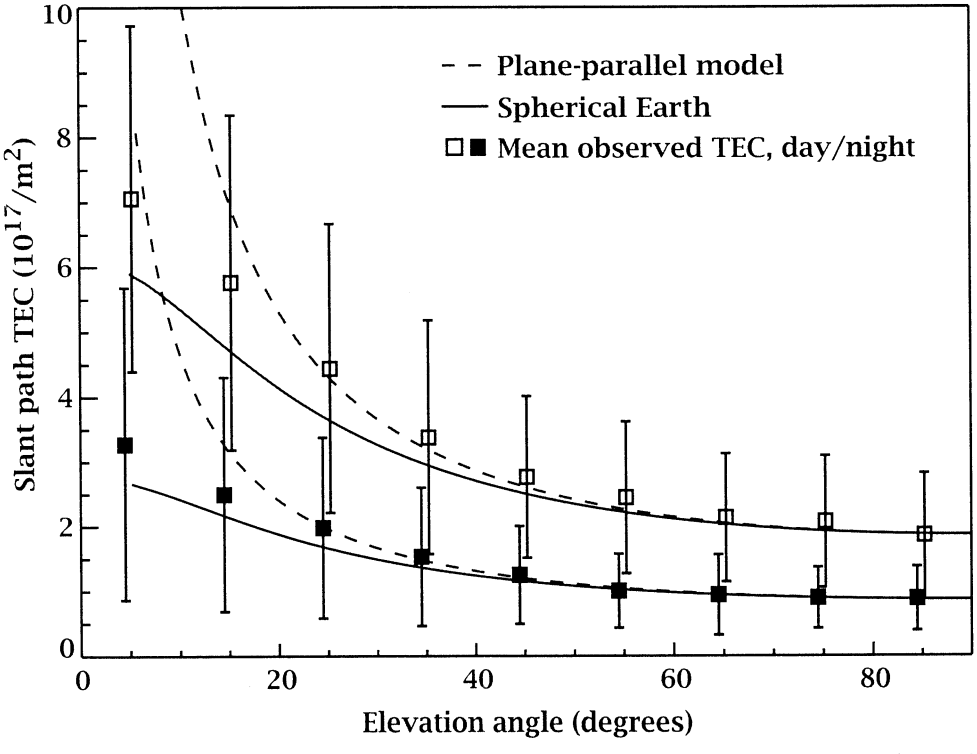

Figure 3. Comparison of actual values of slant path total electron content (TEC) as observed by FORTE with the modeled values, versus elevation angle. The squares represent mean values of slant path TEC for the FORTE data and were calculated for 10° increments of elevation angle. This was done for both night (lower row of squares) and day (upper row). For the plane-parallel and spherical Earth models, we have assumed a constant $N_e t$ value of 0.8×10^{17}/m^2 for night, and 1.8×10^{17}/m^2 for day.

and day. The elevation angles were calculated using the source and satellite positions for these located events. The values of slant path TEC were derived from the observed frequency dispersion, equation (1). The mean values of slant path TEC were calculated for elevation angle intervals of 10° and are plotted as squares (Figure 3). The solid squares represent values of slant path TEC for events recorded at night and the open squares represent those at day. Events recorded at a local satellite time between 0700 and 1700 were identified as daytime observations. By "night" we mean that the events were recorded between 2100 and 0400 local satellite time. Here 3419 of the prompt coincidences are members of the day population and 7775 are members of the night population.

We now compare the mean behavior of the data to our two models. The values of $N_e t$, or vertical TEC, for night and day can be approximated by the values at high satellite elevation angle. For daytime this value is about, and for night the value is $0.8\times10^{17}/m^2$. We use these two values and (2) and (3) to show the behavior of the two models as a function of satellite elevation angle. For the spherical Earth model the height of the ionosphere is taken to be 300 km. This is an average value for the dominant F layer. The two solid curves in Figure 3 represent the spherical Earth model for day and night. The dashed curves represent the plane-parallel model. The plane-parallel model matches both the day and night data fairly well for elevation angles between about 20° and 90°. For the data and the plane-parallel model, at day, we can expect to see a range of TEC values of about 1.8 to $5.4\times10^{17}/m^2$ for this elevation angle range. The spherical Earth model only covers a TEC range from 1.8 to $4.3\times10^{17}/m^2$ for the same range in elevation angle. Note that for a fixed value of vertical TEC the slant path TEC is always smaller in the spherical Earth model because the complement of δ_i is always larger than the elevation angle. In other words, the slant path through the ionosphere in the spherical Earth model is always smaller than in the plane-parallel model.

Neither model matches the mean values of the data for elevation angles lower than about 20°. At these low elevation angles the standard deviation from the mean data values is also the greatest. One problem is that at low elevation angle, refraction and geomagnetic splitting can become important corrections to (1). Also, we might expect there to be a bias in the data toward low values of slant path TEC at low elevation angle. This will limit our ability to locate storms at low elevation angle.

4.2. Variation in TEC With Latitude

For each satellite observation run, we would like to pick one appropriate value of vertical TEC to represent the local conditions of the ionosphere. Each observation run usually covers about 10 min of time, and the satellite nadir coordinates can change by about 20° in latitude or longitude. Because we know that the vertical TEC is a function of latitude, we now investigate how much we can expect the vertical TEC of the ionosphere to vary with a change in satellite latitude of about 20°.

We estimate the vertical TEC as a function of satellite latitude for day and night. For each prompt coincidence we have a ground location, satellite position, and value of slant path TEC derived from the FORTE data record. Thus we can calculate a value of vertical TEC for each prompt coincidence using the two models. For this calculation we include data recorded at satellite elevation angles of greater than 15°. This reduces the number of prompt coincidences recorded at day and night to 2575 and 5432 events, respectively. The mean values of vertical TEC are plotted as circles and are calculated for data within 5° latitude intervals (Figure 4). The data were recorded during the months of April to September of 1998 and for satellite longitudes near the relaxed-criterion observation range of the NLDN. The mean values represent not only a time of day and latitudinal average, but also a seasonal average. The standard deviations in vertical TEC are plotted as error bars. Both the day and night plots show a slow decrease in TEC with increasing latitude when fitted with a line. However, at day maximum values of vertical TEC are attributed to satellite latitudes near 15-20°.

Figure 4 shows that, on average, there is a slight change in vertical TEC as a function of satellite latitude during both day and night. During the day, for a change in satellite latitude of about 20°, we can expect the average change in vertical TEC to be about $0.6\times10^{17}/m^2$. At night, for the same change in satellite latitude, the change in vertical TEC can be as much as about $0.3\times10^{17}/m^2$.

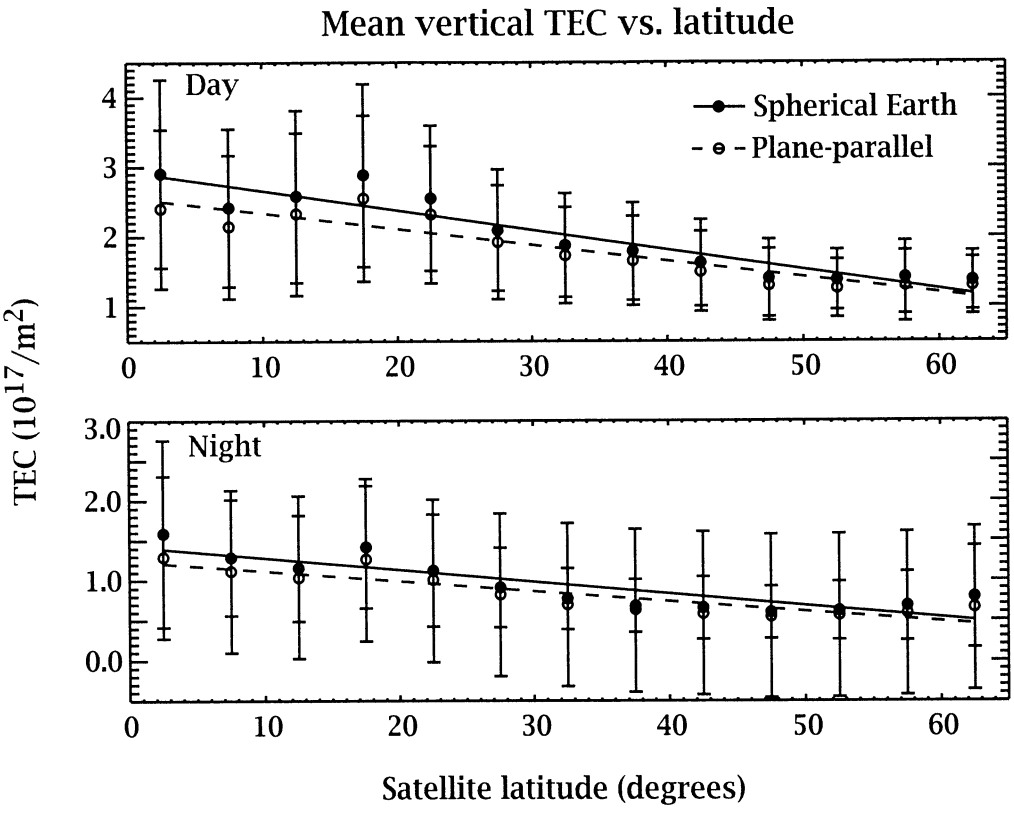

Figure 4. Using the geolocations and values of slant path TEC for the prompt coincidences, we have calculated the approximate vertical TEC at the position of the satellite for both day and night. The mean value of vertical TEC is calculated for each 5° interval of latitude between 0° and 65° using both a spherical and a plane-parallel model of the ionosphere. These values represent a seasonal average for the months of April-September of 1998.

4.3. Recurring Emission Storms

Figure 5 is an example of a plot of TEC versus time in which the satellite data records cluster together in a curve. Each diamond represents one 400-μs data record. The data records circumscribed by squares are promptly coincident with events located by the NLDN. Well-defined clusters, such as these, often indicate that the storm activity is isolated. We first show that given only a median value of vertical TEC, the two models can predict the change in slant path TEC as a function of time for such a satellite observation.

We calculate the elevation angles for the prompt coincidences using the locations of their NLDN counterparts and the time-corresponding positions of the satellite. Since the slant path TEC is also known, we calculate the values of $N_e t$ for these prompt coincidences using (2) and (3). For the spherical Earth and plane-parallel models the median values of vertical TEC are 0.95×10^{17}/m^2 and 0.83×10^{17}/m^2, respectively. For a source location we use the median of the coordinates for the prompt coincidences which are 29.39° latitude and –85.15° longitude. Using (2) and (3), we calculate the slant path TEC as function of the time-dependent elevation angle for both models. These values are plotted as solid and dashed curves in Figure 5. The change in slant path TEC as the satellite moves by the storm is fairly well represented by the curves, indicating that the location of the storm is consistent with the observed change in slant path TEC. The scatter in the FORTE data of Figure 5 is primarily a result of the uncertainty in deriving a TEC value. In addition, for a given satellite position, each signal takes a slightly

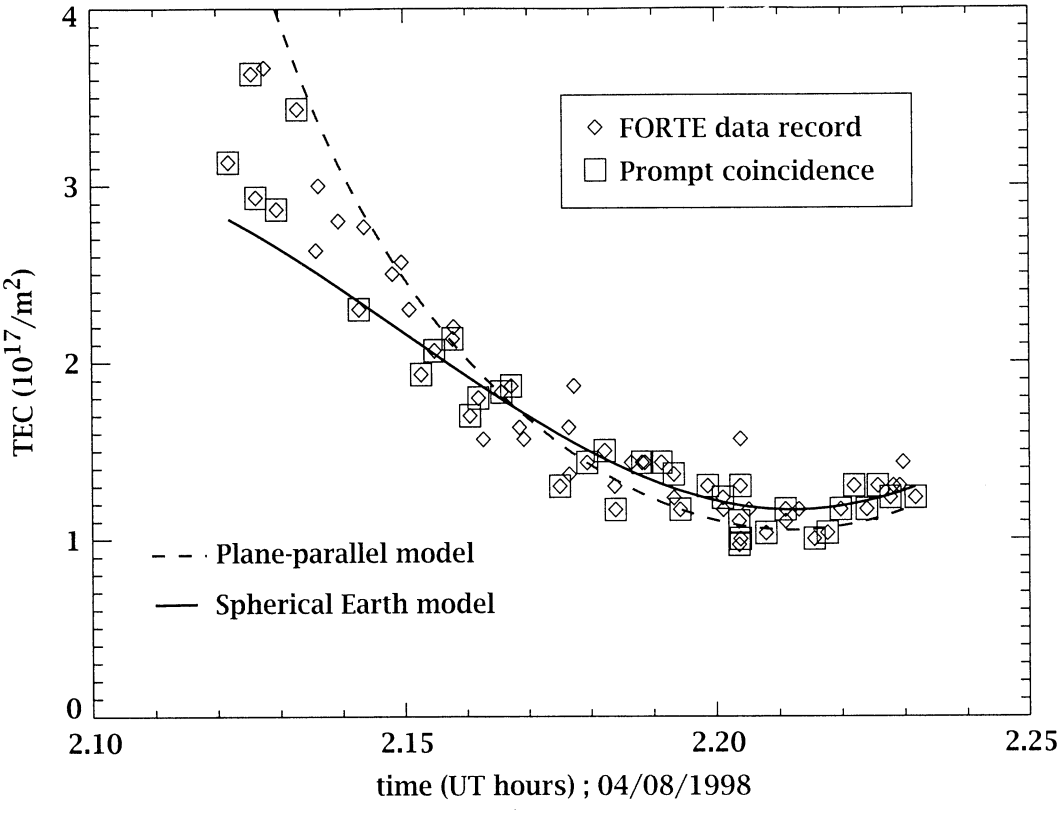

Figure 5. The values of TEC, calculated from the dispersion of FORTE data records, are plotted as a function of time. For the prompt coincidences in this plot, the median values for latitude and longitude are 29.39° and -85.15°, respectively. Using these coordinates for the source location and a median $N_e t$ value of 0.83×10^{17}/m^2 calculated using Eq. 2, we have modeled the expected slant path TEC as a function of time. This is plotted as a dashed curve. The value of $N_e t$ for the solid curve is 0.95×10^{17}/m^2 and was calculated for the same source location, but using a spherical Earth model.

different path through the ionosphere. The individual source locations vary about the median location, and signals emitted from these different locations will propagate through different amounts of TEC. (The position and approximate size of this storm are shown in Figure 8.)

This example shows that using either the spherical Earth model or the plane-parallel model, we can model the change in the observed values of slant path TEC as a function of time using an appropriate value of vertical TEC. Because a median value of vertical TEC can be calculated using the prompt coincidences for any satellite observation run of interest, it is possible to calculate the expected slant path TEC for events originating from any location on the surface of the Earth.

As in this example, there is a spread of about $\pm0.5\times10^{17}$/m^2 for many TEC clusters that represent isolated storm activity. This is in part because (1) provides only a first-order fit to the dispersion. Because this TEC error is larger than the amount we expect the value of vertical TEC to change with latitude for a 10-min observation run, we do not incorporate a latitudinal change in the vertical TEC into our model. We also do not account for refraction in (1)-(3). This will limit our ability to model the behavior of the slant path TEC at very low elevation angles. At elevation angles higher than 15° we have shown that the plane-parallel model provides a better overall fit to the data in Figure 3. Because of this we will use the plane-parallel model in the following analysis.

5. Method

We model values of the TEC traversed by hypothetical VHF sources that originate at locations given by the relaxed-criteria NLDN data set. This is the same data set, covering the months of April-September of 1998, which was used to locate the prompt coincidences. As described in the previous section, we calculate a median value of vertical TEC for each satellite observation run using the slant path TEC and locations of the prompt coincidences. Then, using the plane-parallel model for the ionosphere, we calculate the theoretical values of slant path TEC for events originating at all of the NLDN locations during each satellite observation run. Plots of slant path TEC versus time for the NLDN locations are compared with the plots of the satellite data. Our goal is to identify TEC clusters of satellite data that can be reliably assigned a median storm location. We first check that two or more storms at different locations, observed by the NLDN, cannot contribute points to a data curve that appears to represent isolated storm activity. Second, we restrict the assignment of a location to groups of satellite data that originate in storms covering no more than ±2.5° in latitude or longitude.

Figure 6a shows the data records from one FORTE observation run represented in a plot of slant path TEC, as derived from the data records, versus time. Diamonds represent each of the events recorded by FORTE. Diamonds circumscribed by squares or circles represent data records that are promptly coincident with events located by the NLDN. In this plot the prompt coincidences circumscribed by squares have assigned locations within the range of 26.74°-28.05° in latitude and −103.49° to −102.40° in longitude. We will refer to this lightning active area as "region A" (see Figure 7). The data records circumscribed by circles are from a different lightning active region, and their locations are plotted within "region B" of Figure 7. The data records in Figure 6a cluster into perhaps two distinguishable curves. These are labeled curve A and curve B. Many of the data records have values of TEC that lie within about $\pm 0.5 \times 10^{17}/\mathrm{m}^2$ of these curves. Almost all of the prompt coincidences from region A lie along curve A. Some appear to lie along curve B, but only near the intersection of the two curves. Notice that in Figure 6a one of these events lies at a TEC of about $8.0 \times 10^{17}/\mathrm{m}^2$. We assume that this prompt coincidence is a member of the 2.5% of "accidental" prompt coincidences or that the TEC determination is wrong. It is relatively clear in this case that the events lying near curve A were produced by one region of storm activity because all of the prompt coincidences agree in location. In many cases, there may be fewer prompt coincidences and one or more accidental prompt coincidences lying along a given curve. Because of this, we plot theoretical values of TEC versus time for the NLDN locations made during each satellite observation run.

Here we test whether the NLDN-modeled TEC shows that only one storm region can produce the events that lie along curve A. A median value of vertical TEC is calculated using the values of slant path TEC and locations for the prompt coincident events in Figure 6a. The slant path TEC that would be traversed by VHF signals originating at the given NLDN locations is found for all NLDN waveforms recorded during this observation period. This modeled slant path TEC is plotted versus time in Figure 6b. Events originating from different regions can be displayed as different colors or symbols. Here each NLDN event is represented by a plus sign. The events that are additionally circumscribed by squares originated in region A of Figure 7, and those circumscribed by circles originated within region B. We can clearly see that the dominant lightning active region that FORTE is expected to observe is region A in Figure 7. If we noticed, using such plots, that two or more NLDN regions could produce the same observed FORTE TEC curve, we did not attempt to assign locations to the FORTE data. Notice that the modeled curve in Figure 6b has less spread than the real TEC curve in Figure 6a. Because the value of $N_e t$ is assumed constant, the varying locations of the NLDN data cause the spread in this curve. An attempt to define the size of the storm using the FORTE TEC values would result in an excessively large estimate.

In plot pairs such as those in Figure 6, FORTE events that appeared to be coming from one source region were selected as candidates to be assigned locations. The selected group of events from Figure 6a are those lying within the curved area abcd. Data groups such as this were selected by defining a best fit curve to the data. Events with TEC values having a maximum TEC deviation of $0.5 \times 10^{17}/\mathrm{m}^2$ from the

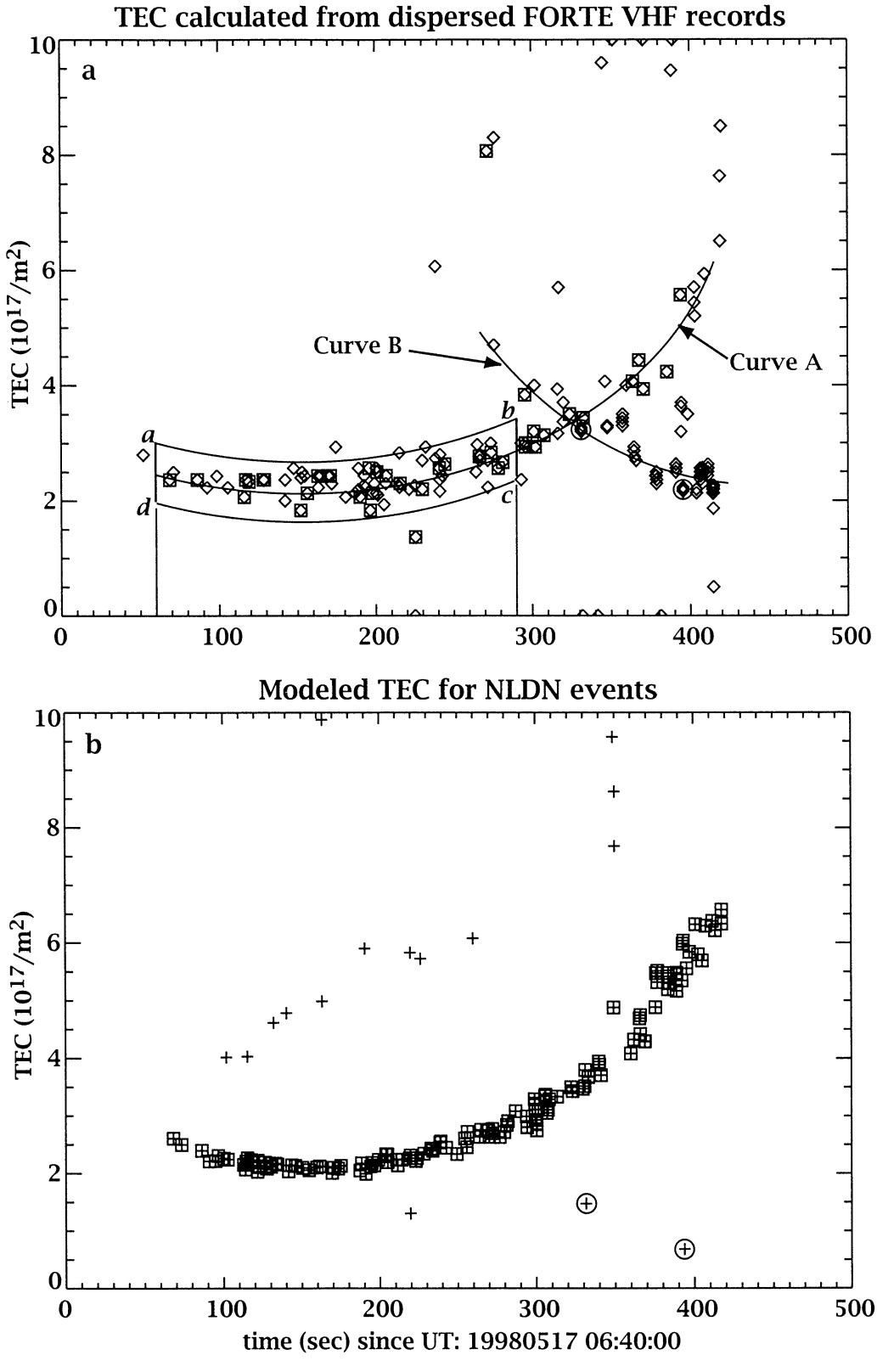
TEC calculated from dispersed FORTE VHF records
a
TEC (10^{17}/m^2)
Curve B
Curve A
a
b
c
d
0
2
4
6
8
10
0
100
200
300
400
500
Modeled TEC for NLDN events
b
TEC (10^{17}/m^2)
time (sec) since UT: 19980517 06:40:00

best fit curve were included. In this example, events near the point of intersection of the two curves were not included in the selection. Events along curve A that were recorded after about 340 s in Figure 6a were not assigned locations. Five of these already have assigned locations because they are prompt coincidences. The other events are at relatively high values of TEC. Events that are assigned high values of TEC often occur quite distant from the satellite. If you consider concentric rings of equal width centered at satellite nadir, rings that are a greater distance from the center cover more surface area of the Earth. At greater distances from the satellite, the probability that more than one lightning region will contribute to events that are assigned similar values of TEC increases. At this point it is possible to assign each nonlocated event in the bounded region abcd in Figure 6a coordinates based on the locations made by the NLDN.

The two events within region B of Figure 7 are those circled in Figure 6. Note that FORTE's detection efficiency of region B is better than that of the NLDN. Many of the events near curve B in Figure 6a may have also emanated from this region. However, these events were not assigned locations because there were only two 0.3-ms events to define curve B. In addition, just before 400 s in Figure 6a, there are some events lying between curve A and curve B that were not coincident with any NLDN events and may indicate that the storm activity near region B is more widespread than observed by the NLDN.

Figure 7 is a map of the events located by the NLDN near FORTE during the observation window of Figure 6. Each NLDN event observed during this time is represented by a shaded square. Events represented by solid squares were promptly coincident with FORTE observations. Region A appears to be isolated from other storm activity based on NLDN data. There is evidence that some activity in the surrounding areas may contribute to the VHF events lying within the curve abcd. However, all of the prompt coincidences originated in region A, and this region is particularly active relative to the surrounding activity. Therefore the events lying within the curved area abcd were assigned the median coordinates from the NLDN events within region A. The minimum and maximum NLDN coordinates within the rectangular boundary were used to estimate the size of the lightning active region during FORTE's transit. In this case, 45 events, which previously had no estimated location, are assigned a median storm location.

The selection of region A and region B as the main producers of the VHF activity observed by FORTE in Figure 6a is consistent with the change in the plotted TEC values in time and the change in the satellite position in time. When the satellite is at closest approach to region A (dashed line), it is about one-third through the observation run, which corresponds to the time of about 190 s. As expected, the observed values of TEC reach a minimum near this time. As the satellite continues to move away from the square bounded storm region, the TEC values for events lying near curve A increase. During this time the satellite is getting closer to region B and the TEC assigned to events lying near curve B decreases. This storm region is farther outside the standard observation region of the NLDN than region A. Thus the detection efficiency of the NLDN is reduced for this region relative to region A. Finally, notice that the circled data points in Figure 6a lie at higher values of TEC than what was modeled in Figure 6b. The vertical TEC was calculated using data from a prompt coincidence of region A. Because the elevation angle is low, the slant path is long and the value of vertical TEC which is a good fit for region A is underestimated for region B. Region B is at a lower latitude than region A. Thus we might have better modeled the TEC

Figure 6. In Figure 6a a diamond represents each FORTE data record. Two symbols, squares and circles, overlie prompt coincidences with NLDN observations from two separate, spatially limited regions. Curve A and curve B are drawn to illustrate the actual time dependence of the slant path TEC for signals originating at these two locations. Events bounded by the curved area abcd were assigned locations. Figure 6b shows the TEC modeled for NLDN events occurring within the FORTE observation window of Figure 6a. Using the plane-parallel model for the ionosphere, each event that was assigned a TEC of $10.0 \times 10^{17}/m^2$ or less, based on the satellite and storm locations, is plotted as a plus sign. Events overlain by squares and circles are from the same two regions as those in Figure 6a.

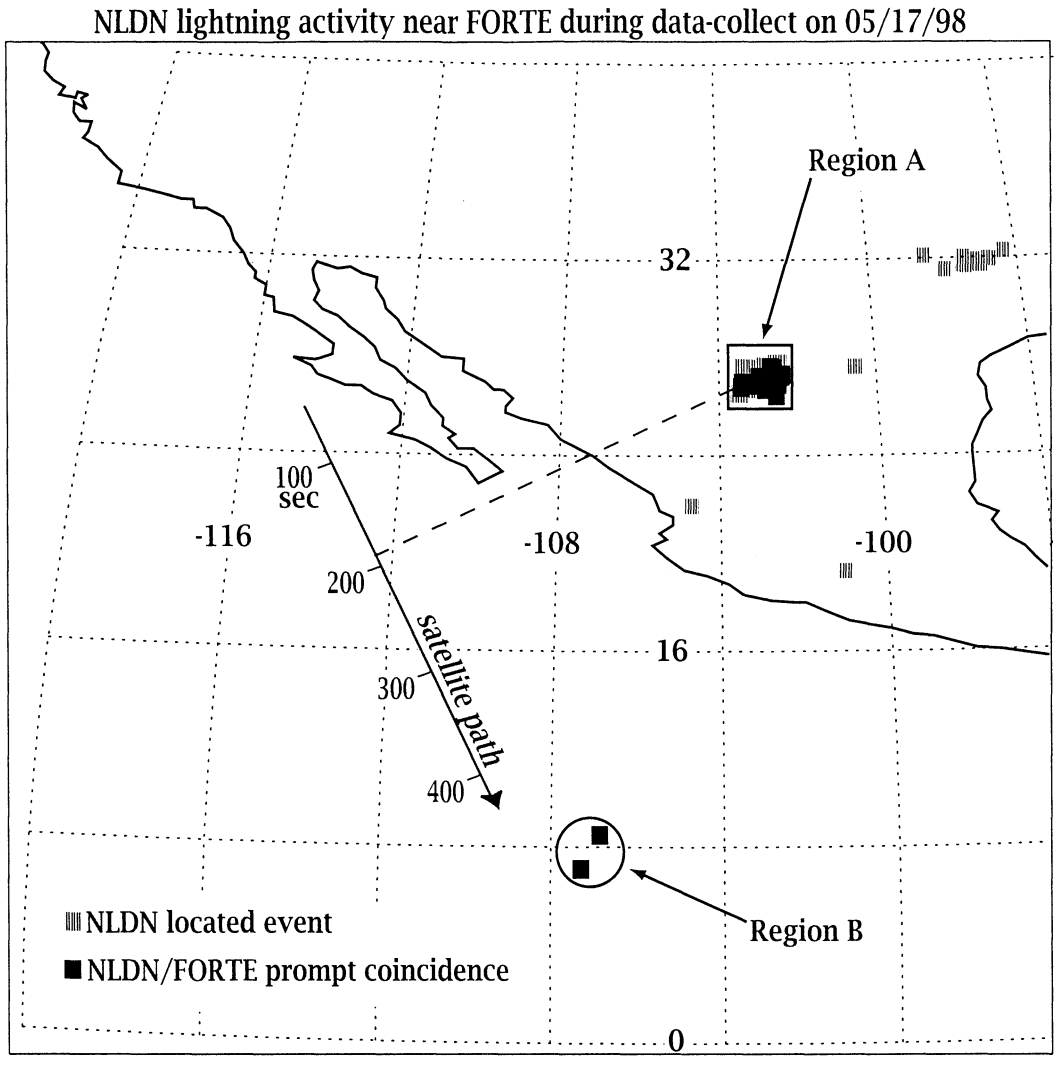

Figure 7. Locations of events recorded by the NLDN near the satellite for the observation window of Figure 6 are shown. Region A is the probable source location for the events lying on or near curve A in Figure 6a, while region B is that for curve B. The satellite position as a function of time for the observation window of Figure 6 is plotted.

versus time for region B by including a latitudinal variation in TEC in our model. We are able to tell, nonetheless, through examination of Figures 6a and 6b, where events from region B begin to contaminate the TEC cluster from region A.

6. Results

The above procedure was carried out for each satellite observation run during the months of April through September of 1998. For this time period we were able to assign approximate locations to 65 groups of data records, such as the group within the curved area abcd of Figure 6a. Twenty-five of these storms occurred during the day, and forty occurred at night. The centers of the crosses in Figure 8 represent the median coordinates of the storms that we identified as the sources of the 65 groups. For the time that FORTE observed a given group, the minimum and maximum of the latitudes and longitudes observed by the NLDN were recorded. These coordinate extremes define the limits of the

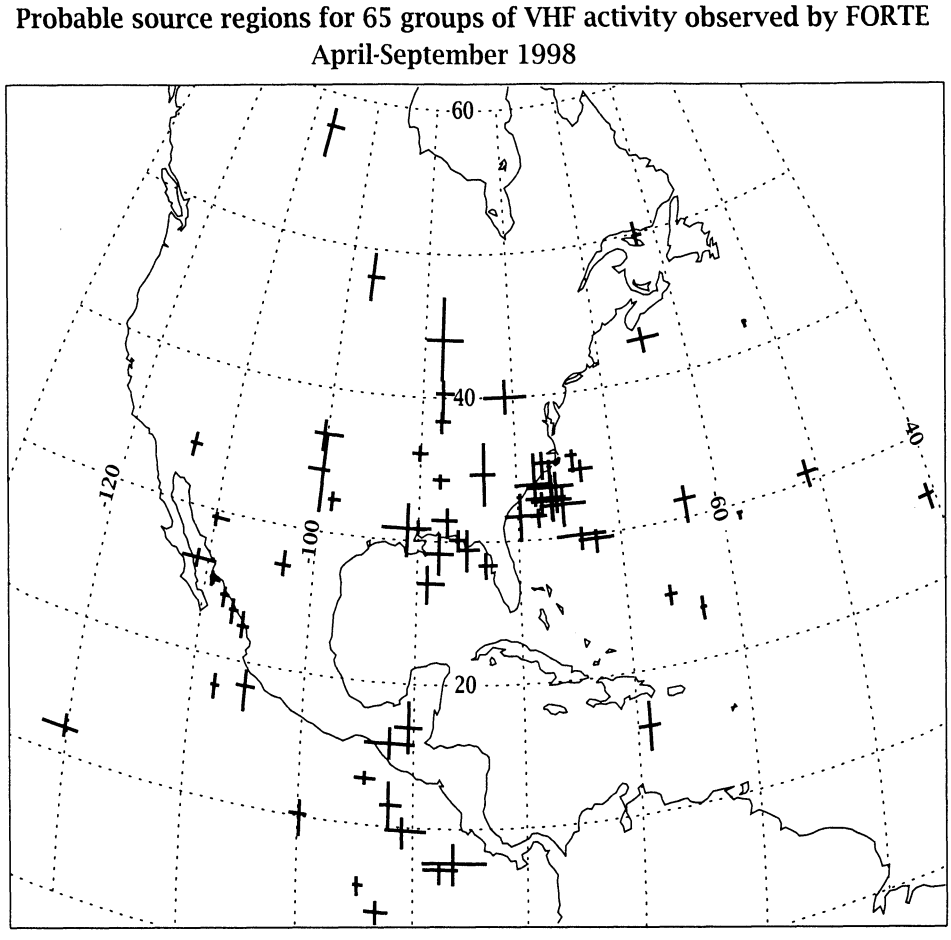

Figure 8. Each cross represents a thunderstorm region that was determined to be the source of a group of VHF data records observed by FORTE. The center of each cross represents the median value of latitude and longitude for the events located by the NLDN during FORTE's observation of the same storm. The ends of the cross arms are the extreme latitudes and longitudes recorded by the NLDN during these time periods. The 65 storms cover continental, coastal, and maritime regions.

cross axes. We were able to locate events from 17 continental, 19 coastal, and 29 maritime storms. We define continental storms as those occurring entirely over land. Coastal storms are those having at least one event located over land and one event located over water. Maritime storms are those in which all located events occurred over water. Though there are a relatively large number of groups of lightning activity that we identify as maritime storms, many of these occurred near the coast. Only a few of these storms were observed far from land. The NLDN recorded much more lightning activity over land than what is represented in Figure 8. Many of the satellite data recorded over land were not located because there was simply too much lightning activity to distinguish one source from another using the TEC plots. Of the TIPPs that were assigned approximate locations in this study, 481 occurred over land, 1038 occurred over sea, and 948 occurred within storms that have been determined to be coastal. About 81% of the TIPPs occurred over coastal or maritime regions, while 74% of the located groups of satellite events occurred over coastal or maritime regions. These numbers are in rough agreement and suggest that TIPPs are just as likely to occur over land as over water.

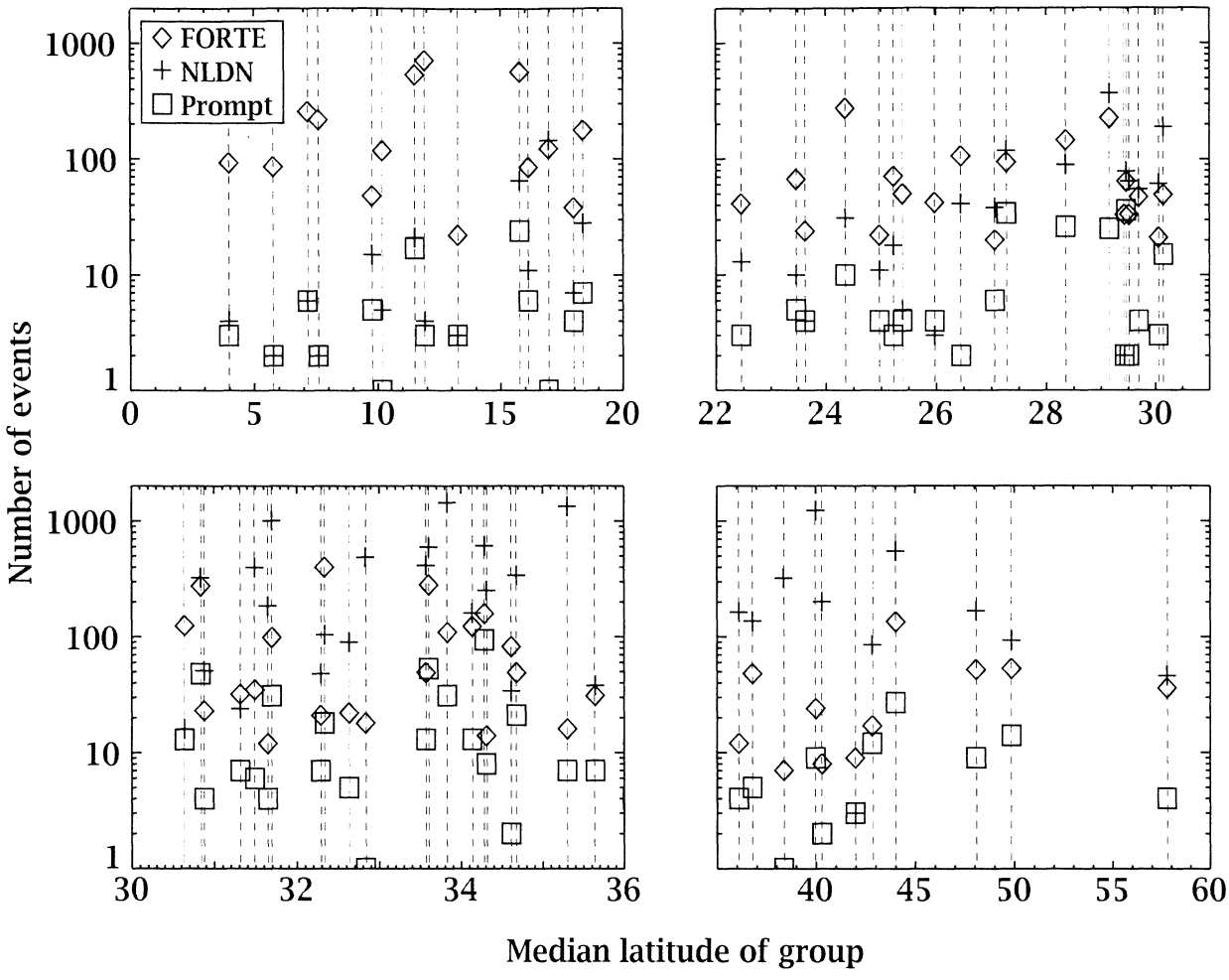

Figure 9. For each of the 65 groups we plot the number of events observed by FORTE and the NLDN and the number of these events that are prompt coincidences. The numbers are plotted versus the median latitude of the storm that was determined to be the source of the event group observed by FORTE.

Figure 9 shows the number of events involved in each group selection by type for the 65 probable source locations. Diamonds, plus signs, and squares represent the number of observations made by FORTE, the NLDN, and the number of prompt coincidences. These numbers are plotted versus median storm latitude. The number of FORTE data records that gained locations using the method described above is the number of FORTE observations minus the number of prompt coincidences. There are a few cases in which FORTE observes a storm very efficiently that the NLDN does not. In these cases the storm is on the outer limits of NLDN's long-range detection capabilities. The true spread of the storm during the observation window could not be determined from the NLDN data in these cases. The most reliable assignments of locations using this method were made for groups containing a large number of both FORTE and NLDN-observed events. This situation occurred often within the latitude range for which the detection efficiency of the NLDN is high.

7. Summary and Discussion

We have described one method of using total electron content to help identify the sources of satellite-observed VHF signals. Storms from

different geolocations within a satellite footprint will often have TEC values that are different enough such that they form distinguishable clusters in plots of TEC versus time. In the present case a subset of the signals had already been assigned NLDN locations using time coincidence statistics. Because the located satellite signals also had a value of TEC attributed to them, we were able to estimate the vertical TEC of the ionosphere using a simple model. This model allowed us to compute the TEC for hypothetical VHF sources originating at NLDN locations. This proved helpful because for every TEC cluster of satellite data that appeared to represent an isolated storm, we could verify that only one storm observed by the NLDN could produce the cluster.

Sixty-five groups of VHF signals recorded by FORTE were assigned geolocations using the method described above. These groups represent a total of 6892 data records. Of this total, 761 had previously been assigned geolocations using timing coincidences with NLDN-located events. Thus, when information on the ionospheric TEC traversed was added to the time coincidence requirement, 6131 additional VHF signals were assigned locations. The 6131 events, to which source locations could be attributed by the process explained here, were recorded by FORTE during the period of April-September, 1998. To extract any more events for which source locations might be estimated could not be done reliably using this method alone. Storm activity is vigorous during these months at northern latitudes. In most cases, storms covered very large areas and no uncontaminated sections of curves could be defined in the plots of TEC versus time. This problem may be improved by including higher-order corrections in the calculation of TEC (equation (1)). Researchers at LANL are currently pursuing the use of GOES satellite imagery and a more detailed model of the ionosphere to assign geolocations to VHF signals observed from orbit.

In future work we will examine the located VHF signals to look for any geographic trends in their characteristics. For the TIPPs that were assigned approximate locations in this study, we will test whether there are any significant differences in the ratio of the power in the second pulse to that in the first pulse for the continental, maritime, and coastal populations. With this data set, it is also possible to examine the VHF records for the signatures of return stroke, subsequent return stroke, and cloud discharge. Taking into consideration the detection efficiency of the satellite, the relative percentage of these event types could be compared for different geographic regions. This sort of analysis will be most useful for satellite signals recorded outside of areas that are efficiently covered by ground-based networks.

Acknowledgments. The authors gratefully acknowledge the FORTE operations team, without whose dedication and hard work the VHF data would not have been available. Joseph T. Fitzgerald and Phillip Klingner are thanked for their helpful suggestions. The NLDN data were supplied by Global Atmospherics, Inc. (GAI), and we acknowledge the support of Ken Cummins of GAI, especially with regard to the relaxed-criterion data. Heidi Tierney is a candidate for the Ph.D. degree in Physics at the University of Oklahoma. In addition to support by DOE at LANL, she has been supported in part by USAF AFSOR AASERT grant F49620-97-1-0410, Paul Bellaire, program director, and in part by the NSF Physical Meteorology Program, grant ATM98-07179, Rod Rogers, program director.

References

Budden, K.G., *The Propagation of Radio Waves*, 667 pp., Cambridge Univ. Press, New York, 1988.

Cramer, J.A., and K.L. Cummins, Long-range and trans-oceanic lightning detection, in *11th International Conference on Atmospheric Electricity Proceedings*, pp. 250-253, NASA Cent. for Aerosp. Inf., Linthicum Heights, Md., 1999.

Cummins, K.L., M.J. Murphy, E.A. Bardo, W.L. Hiscox, R. Pyle, and A.E. Pifer, A combined TOA/MDF technology upgrade of the US National Lightning Detection Network, *J. Geophys. Res.*, *103*(D8), 9035-9044, 1998.

Holden, D.N., C.P. Munson, and J.C. Devenport, Satellite observations of transionospheric pulse pairs, *Geophys. Res. Lett.*, *22*(8), 889-892, 1995.

Jacobson, A.R., S.O. Knox, R. Franz, and D.C. Enemark, FORTE observations of lightning radio-frequency signatures: Capabilities and basic results, *Radio Sci.*, *34* (2), 337-354, 1999.

Jacobson, A.R., K.L. Cummins, M. Carter, P. Klingner, D. Roussel-Dupré, and S.O. Knox, FORTE radio-frequency observations of lightning strokes detected by the National Lightning Detection Network, *J. Geophys. Res.*, *105*(D12), 15,653-15,662, 2000.

Le Vine, D.M., Sources of the strongest RF radiation from lightning, *J. Geophys. Res.*, *85*(C7), 4091-4095, 1980.

Massey, R.S., Ionospheric group delay and phase

including refractive effects, Los Alamos Sci. Lab., *Tech. Rep. LA-11878-MS*, Los Alamos, N.M., 1990.

Massey, R.S., and D.N. Holden, Phenomenology of transionospheric pulse pairs, *Radio Sci.*, *30*(5), 1645-1659, 1995.

Massey, R.S., D.N. Holden, and X.-M. Shao, Phenomenology of transionospheric pulse pairs: Further observations, *Radio Sci.*, *33*(6), 1755-1761, 1998.

Roussel-Dupré, R., and A.V. Gurevich, On runaway breakdown and upward propagating discharges, *J. Geophys. Res.*, *101*(A2), 2297-2311, 1996.

Smith, D.A., Compact Intracloud Discharges, University of Colo., Boulder, 1998.

Suszcynsky, D., M.W. Kirkland, P.E. Argo, R.C. Franz, A.R. Jacobson, S.O. Knox, J.L. Guillen, J.L. Green, and R. Spalding, Thunderstorm and lightning studies using the FORTE optical lightning system (FORTE/OLS), in *11th International Conference on Atmospheric Electricity Proceedings*, pp. 672-675, NASA Cent. for Aerosp. Info. Linthicum Heights, Md., 1999.

Weidman, C.D., and E.P. Krider, The radiation field waveforms produced by intracloud lightning discharge processes, *J. Geophys. Res.*, *84*(C6), 3159-3164, 1979.

Willett, J.C., J.C. Bailey, and E.P. Krider, A class of unusual lightning electric field waveforms with very strong high-frequency radiation, *J. Geophys. Res.*, *94*(D13), 16,255-16,267, 1989.

Zuelsdorf, R.S., C. Casler, R.J. Strangeway, C.T. Russell, and R.C. Franz, Ground detection of transionospheric pulse pairs by stations in the National Lightning Detection Network, *Geophys. Res. Lett.*, *25*(4), 481-484, 1998.

P.E. Argo, A.R. Jacobson, and H.E. Tierney, Los Alamos National Laboratory, Los Alamos, NM 87545. (hmorris@lanl.gov)

W.H. Beasley, School of Meteorology, University of Oklahoma, Norman, OK 73019.

(Received September 14, 1999; revised July 7, 2000; accepted August 22, 2000.)